Development of Cortical Shape in the Human Brain from 6 to 24 Months of Age via a Novel Measure of Shape Complexity

Sun Hyung Kim[a,b], **Ill Woo Lyu**[c], **Vladimir S. Fonov**[d], **Clement Vachet**[e], **Heather C. Hazlett**[a], **Rachel G. Smith**[a], **Joseph Piven**[a], **Stephen R. Dager**[f], **Robert C. McKinstry**[g], **John R. Pruett Jr**[h], **Alan C. Evans**[d], **D. Louis Collins**[d], **Kelly N. Botteron**[h], **Robert T. Schultz**[i], **Guido Gerig**[j], **Martin A. Styner**[a,b,c], and **The IBIS Network**

[a] Carolina Institute for Developmental Disabilities, University of North Carolina at Chapel Hill, USA

[b] Department of Psychiatry, University of North Carolina at Chapel Hill, NC, USA

[c] Department of Computer Science, University of North Carolina at Chapel Hill, NC, USA

[d] McConnell Brain Imaging Center, Montreal Neurological Institute, Montreal, QC, Canada

[e] Scientific Computing and Imaging Institute, University of Utah, Salt Lake City, UT, USA

[f] Department of Radiology, University of Washington, Seattle, USA

[g] Department of Neuroradiology, Washington University, St. Louis, USA

[h] Department of Psychiatry, Washington University School of Medicine, St. Louis, USA

[i] Department of Pediatrics, Perelman School of Medicine at the University of Pennsylvania, Philadelphia, PA, USA

[j] Tandon School of Engineering, Department of Computer Science and Engineering, NYU, New York, USA

Abstract

The quantification of local surface morphology in the human cortex is important for examining population differences as well as developmental changes in neurodegenerative or neurodevelopmental disorders. We propose a novel cortical shape measure, referred to as the 'shape complexity index' (SCI), that represents localized shape complexity as the difference between the observed distributions of local surface topology, as quantified by the shape index (SI) measure, to its best fitting simple topological model within a given neighborhood. We apply a relatively small, adaptive geodesic kernel to calculate the SCI. Due to the small size of the kernel, the proposed SCI measure captures fine differences of cortical shape. With this novel cortical feature, we aim to capture comparatively small local surface changes that capture a) the widening versus deepening of sulcal and gyral regions, as well as b) the emergence and development of

Corresponding author: Sun Hyung Kim, Tel: 919 843 1092, shykim@email.unc.edu.
Present/permanent address:
355 Medical School Wing C, University of North Carolina at Chapel Hill, NC, 27599, USA

secondary and tertiary sulci. Current cortical shape measures, such as the gyrification index (GI) or intrinsic curvature measures, investigate the cortical surface at a different scale and are less well suited to capture these particular cortical surface changes. In our experiments, the proposed SCI demonstrates higher complexity in the gyral/sulcal wall regions, lower complexity in wider gyral ridges and lowest complexity in wider sulcal fundus regions. In early postnatal brain development, our experiments show that SCI reveals a pattern of increased cortical shape complexity with age, as well as sexual dimorphisms in the insula, middle cingulate, parieto-occipital sulcal and Broca's regions. Overall, sex differences were greatest at 6 months of age and were reduced at 24 months, with the difference pattern switching from higher complexity in males at 6 months to higher complexity in females at 24months. This is the first study of longitudinal, cortical complexity maturation and sex differences, in the early postnatal period from 6 to 24 months of age with fine scale, cortical shape measures. These results provide information that complement previous studies of gyrification index in early brain development.

Keywords

Shape Complexity Index; Shape Index; Earth Mover Distance; Age Effect; Sexual Dimorphism

Introduction

Many quantitative brain morphometric measurements, such as regional volumes (Holland et al., 2014; Koran et al., 2014; Lange et al., 2015; Marcus Jenkins et al., 2013; Sowell et al., 2002), cortical thickness, and surface area (Hudziak et al., 2014; Sowell et al., 2004; Storsve et al., 2014; Zielinski et al., 2014) have been used to analyze for brain development, clinical differences, and diagnostic guidelines. These measurements allow for analyses of the global or local developmental trajectory over age, differential anatomical changes, and the relationship between anatomical changes and brain functions or environment factors. As the human cerebral cortex is a highly folded, convoluted object composed of sulci and gyri, the maturation patterns of sulcal and gyral folding have increasingly been studied.

Historically, older studies of cortical folding have focused on global measurements that encompass whole hemispheres, particularly the global gyrification index (GI) measurement, which is defined as the area ratio between the outer cortical surface, such as cerebral hull surface, and the cortical gray matter surface (Armstrong et al., 1995). While global GI measurements have the strong advantage of scale invariance, they generally cannot yield localized measures of complexity. Another global cortical folding measure is the fractal dimension (FD) (Free et al., 1996), which provides information about the inherent scale of the folding in such a complex structure. It has the advantage of being free of a reference smooth surface, such as the cerebral hull for GI, but it has shown to be very sensitive to noise in the surface reconstruction (Free et al., 1996).

More recently, local measurements have emerging due to developing computing technology. The traditional FD analysis used box-counting approach, but that has to assure the subject alignment and normalize of brain size. The spherical harmonic reconstruction reduced the effect of alignment error and brain size variant (Yotter et al., 2011). Also, the cortical

surface's local intrinsic or extrinsic curvatures at each location were proposed as surrogate measures of cortical folding (Gaser et al., 2006; G. Li et al., 2014; K. Li et al., 2010). Both intrinsic (called Gaussian curvature) and extrinsic curvatures (called mean curvature) are fundamental measurements of local surface shape. Intrinsic curvature captures the tangential expansion of the local surface and quantifies the amount of excessive local area compared to the projected area in tangential plane with the sign capturing whether the local setting is cup-like or saddle-like (Ronan et al., 2014; 2012). Similarly, local sulcal depth (Dierker et al., 2015; Meng et al., 2014; Rettmann et al., 2006) and sulcal length (Kochunov et al., 2010) measures have been suggested for analysis as sulcal depth captures a coarse, simplified measure of folding distance to the cerebral hull in the child and fetal cerebral cortex of primates.

However, the definition of kernel size or window would be issue to perform the local analysis. The local measures of GI have been proposed using a larger sized kernel defined by Euclidean distance (Su et al., 2013) or a quasi-geodesic N-ring neighborhood (G. Li et al., 2014; Schaer et al., 2008). The Euclidean spherical kernel was defined using intersecting locations between the outer surface and a sphere of fixed radius. For the local GI analysis to be sensible, an adaptive kernel size needs to encompass at least one sulcal or gyral region. Larger sizes were usually chosen, typically larger than 20mm~25mm, which leads to local GI measures that encompass several gyri and sulci within the same kernel. None of the local curvature-based studies known to the authors take into account the overall brain surface size, which affects the density of the cortical surface sampling. Thus, larger brains would generally encompass larger local areas for averaging the curvature within a certain kernel size than smaller brain would. Local GI studies often correct for overall brain size differences. However, the local change of surface area has not been taken into account in longitudinal studies of brain development (G. Li et al., 2014).

Sulcal or gyral patterns analyzed via the above measures may reflect morphological development and pathological functioning associated with neuropsychiatric disorders, such as autism and schizophrenia (Lui et al., 2011). The development of morphological folding is apparent from approximately 16 weeks of gestational age and develops into an increasingly complex folding pattern into the early childhood period (Armstrong et al., 1995; Wright et al., 2014; ZILLES et al., 1988). While the predominant view is one of consistent increase in cortical folding complexity, with considerable variability of the exact pattern across different studies, Rettman et al (Rettmann et al., 2006) have reported a decrease in local cortex curvature in the central, cingulate, and parieto-occipital sulcal regions over the first 4-years of human development. The observed diversity of reported results in cortical folding studies may arise from multiple factors, mainly the selection of the measure, as well as the choice of scale. Studies of sulcal depth and local curvature yield measures at a very fine scale, measured just within the immediate neighborhood of a cortical location, whereas studies of local GI yield relatively large scale measures, capturing regions across multiple sulci and gyri, combining regions that may be functionally quite divergent.

In this work, we propose an alternative scale that quantifies the cortical folding via a local complexity metric computed within an intermediate neighborhood size that does not span across multiple gyri or sulci. This novel measure complements the existing set of cortical

folding measures and provides a novel viewpoint to the study of cortical complexity that is relevant for understanding and investigating underlying mechanisms of development in the early postnatal period. This measure is able to distinguish whether a sulcal or gyral region undergoes a widening or deepening process, which would be undistinguishable via local GI measures. Also, we aim with the measure to capture the emergence and development of secondary and tertiary sulci with enhanced localization as compared to GI due to the smaller kernel size. It is furthermore noteworthy that the discussion of the kernel size is often treated with limited consideration. Like intrinsic curvature and GI measures, the novel measure we propose here is susceptible to the choice of the kernel size, which we aim to address via the kernel size normalization. This normalization of the kernel size allows the proposed surface complexity index (SCI) to have invariant results in terms of brain size and also takes into account expected surface area changes in longitudinal studies. In addition, the SCI is directly measureable on surface points without the need of reference surfaces, such as the smoothed or inflated/simplified brain surface needed for the computation of GI. Finally, in a reliability study, we demonstrate the robustness and stability of the SCI measure.

Method

Participants

We studied 202 brain MR images from typically developing subjects with no family history of autism spectrum disorder assessed at 6, 12 and 24 months of age as part of a National Institutes of Health-funded, multi-site, Autism Centers of Excellence (ACE) Network study: the Infant Brain Imaging Study (IBIS). The MRI scans were acquired at 4 different sites (University of North Carolina at Chapel Hill, University of Washington at Seattle, Washington University at Saint Louis and Children's Hospital of Philadelphia) each equipped with 3T Siemens Tim Trio scanners. The scan sessions included T1 weighted (160 sagittal slices with TR=2400ms, TE=3.16ms, flip angle=8, field of view 224×256) and T2 weighted (160 sagittal slices with TR=3200ms, TE=499ms, flip angle=120, field of view 256×256) MRI scans. All datasets possess the same spatial resolution of $1 \times 1 \times 1 mm^3$. We selected the longitudinal MRIs between 6 and 12 months of age and between 6 and 24 months of age in order to normalize the local kernel size. The cohort included 76 scans from female subjects (mean months of age: 12.91 ± 6.74) and 126 scans from male subjects (mean month of age: 12.33 ± 6.35), see Table 1, from a total of 30 female subjects (14 with 2 longitudinal and 16 with 3 longitudinal scans) and 52 male subjects (30 with 2 longitudinal and 22 with 3 longitudinal scans).

A number of quality control procedures were employed to assess scanner stability and reliability across sites, times, and procedures. A Lego (Lego Group, Billund, Denmark) brick based phantom (Fonov et al., 2010).was scanned monthly at each location and analyzed to assess image quality and quantitatively address site-specific regional distortions. In addition, two adult subjects were scanned once per year at each scanner and after any major scanner update. The data for these phantoms were evaluated for scanner stability across sites and time (Gouttard et al., 2008) and are also used here to assess stability for the proposed cortical shape complexity measure.

Image processing and surface generation

The raw MR T1 and T2-weighted (T1w, T2w) images were corrected separately for geometric distortions (Fonov et al., 2010), as well as for intensity non-uniformity (Sled et al., 1998). All T2w images were rigidly registered to their corresponding T1w images via standard mutual information registration using Automatic Nonlinear Image Matching and Anatomical Labeling (ANIMAL) tool (Collins et al., 1994; Fonov et al., 2011). In the case of registration failure, we manually initialized the registration procedure and reran the registration procedure. Afterwards, both T1w and T2w images were rigidly transformed to stereotaxic space based on the registration of the T1w scan (Collins et al., 1994). A prior intensity growth map (IGM) was applied to both T1w and T2w images for 12 month scans to enhance the contrast of the WM/GM boundary due to under-myelination (KIM et al., 2013). Tissue classification, as according to the Atlas-Based Classification (ABC) (Van Leemput et al., 1999) and atlas based multi-modal approach, was performed to obtain white matter (WM), gray matter (GM), cerebrospinal fluid (CSF), and background. For the 12 and 24 month scans, the inner and outer surface models were extracted using an adapted version of the 'Constrained Laplacian-Based Automated Segmentation with Proximities (CLASP)' pipeline (J. S. Kim et al., 2005). The surfaces for 6 month scans were generated by propagating surfaces from corresponding 12 month scans via deformable multi-modal within-subjects co-registration using ANTs (Avants et al., 2008). The cortical surface model consisted of 81,920 high-resolution triangle meshes (40,962 vertices) in each hemisphere. The smoothed middle surface was obtained by averaging pial and white surfaces and then two iterations of averaging based surface smoothing. Cortical surface correspondence was established via spherical registration to an average surface template, which performs a sphere-to-sphere warping by matching crowns of gyri (Robbins et al., 2004).

Local shape complexity index

To describe the local geometric surface shape, we first employ the well-known surface shape index (SI) (Koenderink and van Doorn, 1992), calculated at each surface vertex on the middle surface using the following equation: $SI_i = (2/\pi) \times \arctan((k_{2,i} + k_{1,i}))$, where i is the vertex index, k_1 and k_2 are the principal curvatures at the i-th vertex on the surface which is calculated by estimating tensor curvature algorithm in order to have a continuous tensor field over the whole surface (Cohen-Steiner and Morvan, 2003). The SI score ranges from −1 to 1 and can be subdivided into 9 standard geometric topological situations at the following values (see also Supplemental Figure S1): spherical cup (SI=−1.0), trough (SI=−0.75), rut/valley (SI=−0.5), saddle rut (SI=−0.25), saddle (SI=0), saddle ridge (SI= 0.25), ridge/crest (SI=0.5), dome (SI=0.75), and spherical dome (SI=1.0). We employed the Stanford bunny model (Figure 1, a) to illustrate the SI map (Figure 1, b) and show the efficient capture of the local geometric shape.

The proposed shape complexity index (SCI) was defined by the quantification of SI variance within a local region. For example, regions that have the homogeneous SIs are considered to have a low complexity, whereas regions that have both convex and concave parts should have a relatively high complexity (see Figure 1, b). For that purpose, we investigated three different ways to quantify the homogeneity of the local SI distribution.

Quantification of the SI distribution

For the quantification of SI homogeneity within a local neighborhood, we computed the histogram of the local SI for all surface vertices within a geodesic distance. We then looked at three measures derived from this SI histogram: a) histogram kurtosis (Hosking, 2006), a measure of the "peakedness" of the distribution, b) histogram (differential) entropy (Stone and Bray, 1995), a information theory based measure of heterogeneity, and c) the discrete Earth Mover's Distance (EMD) (Rubner et al., 2000) between an idealized model of minimally low complexity and observed histogram of SI. The kurtosis is computed via the ratio between the fourth moment around the mean and the square of the variance of the probability distribution. A high kurtosis value represents a sharper peak and a relatively low value represents a more rounded peak of histogram (Figure 2, a). The entropy can be estimated via the histogram bin counts (Figure 2b). Recently Lefevre et al's study is based on global statistical analysis using fitted model from the observed distribution of measurement (volume, GI, SI, curvness) in each feature (Lefèvre et al., 2015). It is a good approach to summarize corresponding surface measures across subjects, which is likely of Gaussian nature, but it does not capture well the local variability of the SI distribution within a given surface, which is often non-Gaussian.

For the discrete Earth Mover's Distance (EMD) based complexity measure, we calculate the difference of the actual observed SI distribution compared to the best fitting, idealized distribution of a maximally simple (non-complex) geometric setting (see Figure 3). The EMD at each vertex is computed for all 9 ideal basic settings and the minimal EMD at each vertex is chosen as its complexity measure.

The EMD represents a metric that captures the minimal cost that must be paid to transform one distribution into the other via linear optimization (Rubner et al., 2000). For the computation of this measure, let $P_v = \{(p_1, w_{p1}), (p_2, w_{p2}), \ldots, (p_9, w_{p9})\}$ be the histogram of SIs distribution with 9 bins within an adaptive kernel size and $Q_s = \{(q_1, w_{q1}), (q_2 \, w_{q2}), \ldots, (q_9, w_{q9})\}$ be the histogram of the basic 9 geometric settings mentioned before. Where w_{pn}, and w_{qn} is the number that is representative of each bin. v is the vertex index, and s is from 1 to 9 for each basic geometric settings. $p_{1\sim9}$ and $q_{1\sim9}$ is the bin representative, so $\{p_1, \ldots, p_9\}$ and $\{q_1, \ldots, q_9\}$ is $\{-1.0, -0.75, -0.5, -0.25, 0, 0.25, 0.5, 0.75, 1.0\}$. And the 9 histograms of different geometric setting are made using same number of vertex on each observed P_v, so $\sum_{i=1}^{9} w_{p_i} = \sum_{j=1}^{9} w_{q_j}$.

$$EMD(P,Q) = \frac{\sum_{i=1}^{m}\sum_{j=1}^{n} d_{ij} f_{ij}}{\sum_{i=1}^{m}\sum_{j=1}^{n} f_{ij}}, (m, n=9)$$

where f_{ij} is the flow between the elements of observed p_i and the elements of basic geometric setting q_j The distance d_{ij} is calculated by the absolute difference between the histogram elements, i.e. the SI measures. The minimized amount of flow f is calculated by solving the linear programming problems in cost function with following conditions.

$$f_{i,j} \geq 0, (1 \leq i \leq 9, 1 \leq j \leq 9)$$
$$\sum_{i=1}^{9} f_{i,j} \leq w_{q_j}, 1 \leq j \leq 9$$
$$\sum_{j=1}^{9} f_{i,j} \leq w_{p_i}, 1 \leq i \leq 9$$
$$\sum_{i=1}^{9} \sum_{j=1}^{9} f_{i,j} = \sum_{j=1}^{9} w_{q_j}$$

The EMD for SI histograms, which range from −1 to 1, is maximally bounded at 2. As we are searching for the minimal EMD over selected geometric settings, it can be shown (independent of the granularity of the selected geometric settings employed) that the EMD is maximally 1 (maximal EMD is achieved when the observed distribution is balanced and bimodal at the SI extrema of 1 and −1).

$$SCI_v = min\left(EMD\left(P_v, Q_s\right)\right), s \in \{1, 2, \ldots, 9\}$$

The one histogram among the 9 histograms of geometric setting would be best representative to reveal the homogeneity of obtained SIs within an adaptive kernel size. That histogram matches up the peak of the histogram of obtained SIs. Therefore, the SCI_v on each vertex is decided after calculating minimum EMD between the observed P_v histogram and the histogram of 9 different geometric settings.

Figure 2 shows a comparison of the 3 measures on an example surface. While a good overall correlation across the measures is visible, there are predominant differences. The kurtosis results indicate a measure that is noisier than the other two measures. The entropy results show a ceiling effect that results in a limited dynamic range for areas of higher complexity. The whole brain histogram of the entropy measure, not surprisingly, tends to be skewed to the right side. The EMD based complexity measure looks smoother across the brain than the other measures and seems to have a high dynamic range. The whole brain histogram of the EMD measure indicates a symmetric, near Gaussian distribution. These observations lead us to choose the EMD based measure for our quantification of a local shape complexity index/ SCI.

Adaptive kernel size

The SCI is based on the distribution of the shape index within a given neighborhood/kernel. As such, the SCI is relatively sensitive to the choice of kernel size. As the mesh cannot be considered perfectly sampled in a uniform way, we use local geodesic distances for the SI histogram computation. Figure 4 illustrates the size of local geodesic kernels at various (randomly sampled) cortical locations for an example surface of a 6-month-old subject. For a kernel size over approximately 5mm, several cortical locations would sample both gyral ridges and sulcal fundi. As we aim to compute a local surface complexity metric that remains within a sulcus or gyrus, we made the decision to employ a kernel size that does not cover both sulci and gyri within the same kernel. Given the visualization in Figure 4, we chose 3mm as the 'empirical fixed kernel size' (KIM et al., 2015). Other kernel size choices

(e.g. 2.5 ~ 4.0 mm) would be valid, though such different choices would change the nature of the computed SCI and its biological interpretation. Experimental results presented later (see Figure 5) indicate that a kernel size of 3mm is a good choice, with respect to the dynamic range of the computed SCI. The last column of Figure 5 has been extended to include also a kernel size of 8mm, which captures such neighboring folds within a single kernel. The results indeed show that our proposed SCI is sensitive to such an enlargement of the kernel in that the computed age effects are quite different between a 3mm and 8mm kernel. We expected such a difference, and would not call this a problem, but rather a feature. If one is interested in a measure capturing multiple gyri/sulci then a kernel size of 8mm or larger is suggested. In our work, we set out from the start to create a measurement whose scale captures single gyri/sulci areas, which is why the results in the manuscript focus on a kernel size at 3 mm. While additional analyses at a multi-gyri/sulci kernel size could be done, we have chosen not to perform such analyses given the ceiling effect in the SCI that we observe at 8mm already (see Figure 5a and 5b).

A fixed constant kernel size for brain surfaces of different subjects has the limitation of resulting in an inconsistently sized area at corresponding points due to inter-subject differences in brain surface size, even at the same age (in this case, 6 months). Overall, the total surface area shows the mainly linear growth pattern within the window of our observed age, from 6 months to 24 months (Figure S2 a, Figure S3). Thus we feel a linear correction, while not perfect, is still appropriate. Also, the changes of local surface area show a clear non-uniform pattern, in that the bilateral superior and inferior middle frontal and posterior cingulate have a relatively high increase in surface area, whereas the superior parietal and cuneus actually decreases in surface area. Thus, for an appropriate longitudinal/ developmental study of any kernel based cortical surface analysis, the kernel size should be adapted to take into account the variability of expected change in surface area across different anatomical regions. Thus, an appropriate normalization of the kernel size needs to be adopted. As we are studying longitudinal changes of cortical shape from 6 to 24 months, we chose the youngest time point (6 months) as a reference for the kernel size normalization.

For 6-month-old subjects, we suggest normalizing the hemisphere kernel size globally for the brain surface via the ratio of that subject's brain surface area to the average brain surface area in each hemisphere. The kernel size k_i for the i-th subject at 6 months of age is then computed as follows:

$$k_i = k_{fixed} \times \sqrt{\frac{\sum_j SA_{i,j}}{\frac{1}{N}\sum_n^N \sum_j SA_{n,j}}}$$

where $SA_{i,j}$ is local surface area at vertex j of the i-th surface that is calculated via averaging within one vertex neighborhood, and k_{fixed} is the chosen fixed kernel size of 3mm, and N is the number of subjects. We computed the SCI variations in the presence of simple brain scaling differences from 80% (a) to 120% (c) using a single/same kernel size. The observed differences are smaller than 0.1% of the SCI range across the brain and thus our proposed SCI measure is likely stable in the presence of global scaling/size differences. Furthermore,

we control for global size effects, by incorporating the full brain surface area as a normalization factor of the subject-specific kernel size k_i (Figure S4).

While for subjects of 6-months-old, we calculate the local SCI using the above formula, we chose different normalization methods for older subjects, as the local surface area expansion in brain development has been shown to be non-uniform across the brain (Hill et al., 2010; G. Li et al., 2014).

We use two-time points data set in order to normalize a locally adaptive kernel that takes into account the local developmental brain surface size. The locally normalized kernel size is computed here as the globally normalized kernel scaled with the local surface area ratio at 12 or 24 months versus the one at 6 months. The equation for the local kernel size $k_{i,j}$ for the i-th subject at vertex j at age a =12 or 24 months is then as follows:

$$k_{i,j}^a = k_i \times \sqrt{\frac{SA_{i,j}^a}{SA_{i,j}^{6m}}}$$

This local normalization increases or decreases the kernel size as a ratio of the surface area change, such that for an individual the same local, relative kernel size is longitudinally employed. The left and right mean kernel size is 3.0152 mm (variance: 0.0105mm) and 3.0315 mm (variance: 0.0122mm) in 6 months age. The range of mean at 12 months is between 3.1445 mm and 3.5634 mm and between 3.2545 mm and 4.2412 mm at 24 months. The similar pattern of mean and variance of kernel size shows in 12 and 24 months data (See also Supplemental Figure S5).

Statistical Analysis

All raw SCI maps were first mapped onto the common MNI surface template space (Lyttelton et al., 2007) for further processing and analysis. As a first common step in the analysis of measurements at the cortical surface, we computed a geodesic heat kernel based smoothing of the SCI maps. The smoothing employed a 2.5mm bandwidth and 100 iterations (Chung et al., 2005). The effects of age and sex were tested via a longitudinal mixed effects model in SurfStat, a toolbox for statistical analysis of cortical surface data employing random field theory for statistical inference (Chung et al., 2010). Firstly, the longitudinal linear mixed model with a random intercept and slope was fitted to the data capturing estimates for contributions of age, sex, as well as sex*age interactions, with the following formula:

$$y_i = \beta_0 + \beta_1 \quad sex_i + \beta_2 \quad age_i + \beta_3 \quad age_i{}^* sex_i + \gamma_i$$

where y_i is the dependent variable, SCI, and γ_i is the random effects coefficient for subject i. To correct for the multiple comparisons, we employ standard false discovery rate (FDR) (Benjamini and Hochberg, 1995) for the effect of age and adaptive FDR for the effect of sex (Storey et al., 2004).

Results

Local complexity example

Figure 3 shows two examples of the local SCI measure alongside the local SI histogram distribution and the idealized histogram of its corresponding best fitting basic geometry setting. In this particular example, the selected gyral region, which is close to a gyral top, is more complex than the selected sulcal region as indicated by the higher EMD score (Figure 3, a). The deep sulcal fundus regions, sulcal wall in deep sulcal regions or wide gyral regions tend to have simpler complexity, as expected, whereas the sulcal wall in relatively shallow sulcal regions or the gyral ridge regions show a relatively low SCI score (Figure 3, b). Gyral saddle and gyral ridge regions display an intermediate level of shape complexity.

Reproducibility

We evaluated the stability and reliability of the proposed shape complexity measure using a large set of scan/rescan dataset. Two human phantoms (male, age 26 and 27 at start of this study) were scanned at the four different imaging sites, each equipped with a Siemens 3T Tim Trio scanners for evaluation, at irregular intervals over the period of 2.5 years. The same scanning sequences were employed as for the developmental MRI scans. Overall, this resulted in 35 scan sessions for subject I and 31 scan sessions for subject II. We computed the tissue segmentation, brain surface reconstruction, and SCI maps independently and analyzed the local coefficients of variation (COV) as a measure of stability that is defined by the ratio between the standard deviation and mean: $COV_i = 100 \times \sigma_i/\mu_i$, where i is a number of vertex. This analysis revealed excellent stability with overall across-site COV values below 0.8% for all cortical regions, as well as COV values below 0.3% for most of the brain (see Figure 6). The higher COV values, approximately 0.8%, resulted from the inferior frontal region next to the eyeball, likely due to the variance of the brain mask in that region. It is noteworthy that overall intra-cranial volume measures showed across-site COV just below 1% (Bryson et al., 2008; Hazlett et al., 2012) in this dataset. Therefore, our measure seems to be as stable as computations of such ICV measures, at least in the adult brain.

Local complexity over age

Figure 7 shows t-statistic maps under FDR threshold p<0.001 for the age effect mapped onto the average template surface. Scatter plots at selected regions with regional peaks of significance, as well as regions of non-significance illustrate the local distributions. Local SCI in most brain regions revealed a highly positive correlation with age, except in the bilateral superior frontal, inferior temporal, and lingual gyral regions (a, g), where no significant age correlations were observed. The cerebral cortex showed a larger significant age correlation in the anterior and posterior cingulate (d, f), pre- and post-central gyral region (b), and superior temporal gyral region (c). No cortical regions showed a significantly negative association of age and the local SCI. Figure 8 shows the linear SCI change rates per month between 6 and 24 months of age. While statistically not significant, the left calcarine fissure showed decreasing SCI (cold color regions) at a change rate of SCI is −0.0012 per month. Of those regions with increasing SCI (warm color regions) the largest increase is observed in the left parahippocampal gyrus region (0.0017 per month), with a mean SCI change rate of 0.0005 across the brain. Finally, we observe that the overall distribution of the

age effect and change rates appears largely symmetric across hemispheres, though no analysis of asymmetry is performed here.

Sexual dimorphism of local complexity

Several small cortical regions show higher SCI for male subjects at 6 months of age (shown in red) in cross-sectional analysis (see Figure 9 a). Those regional differences are no longer visible at 12 months, but other regions show the significant differences with some more complex in females (shown in blue) and in males (shown in red) (see Figure 9 b). At 24 months, higher complexity in left lateral prefrontal, occipital and right inferior temporal region is predominant for female (see Figure 9 c). It means the growth pattern of complexity changes during this period.

Figure 10 displays the results of the longitudinal analysis of sex as well as the sex*age interaction. Male subjects show persistently higher complexity in the left insula, visual cortex, superior temporal, right post-central, left posterior ventral cingulate, and parieto-occipital sulcus region (shown in red; a, b, d, e). Female subjects have higher cortical complexity mainly around Broca's regions (shown in blue; c). The difference in sex*age interaction of SCI shows the nearly opposite results comparing the statistical difference of sex, Figure 10 A (Figure 10, B). The longitudinal change of SCI in female subjects is larger than in males in the left insula (a), the left posterior ventral cingulate (d), the parieto-occipital sulcus (e), and the slower in Broca's regions (e). Additional regions, such as the right anterior superior temporal gyrus (f) region, show no significant sex differences, but has a significant age*sex interaction, where the longitudinal change in SCI is larger in male than female subjects.

Sensitivity to kernel size choice

The surface area of the human brain grows rapidly, as well as cortical thickness in the first years of life. Since the cortical surfaces at all time points were generated using the same number of vertices, a fixed kernel size would be expected to yield different results than presented above, leading to differing biological interpretations. Therefore, we chose to investigate the influence of the kernel in more detail, with results presented in Figure 5. The top row shows the calculated SCIs with different global geodesic kernel sizes in a randomly selected 6-month-old dataset. SCIs that are calculated with a small kernel size, 2.5mm, tend to show a ceiling effect with few regions of high complexity and large parts of the brain at relatively low complexity. Results using a larger kernel size (over 3.5mm) show a ceiling effect with few regions of relative low complexity. These effects are even more pronounced following the local smoothing operation (Figure 5 b). A kernel size close to 3mm seems to have the best dynamic range for the proposed SCI.

The local difference of SCI is about 10% when the kernel size is decreasing or increasing by 0.5mm, as seen in the ratio maps in Figure 5 c. More complex regions, such as the pre-/post central region or the superior-/inferior parietal lobes, show a bigger sensitivity to the choice of kernel size, demonstrated by the local magnitude differences in the ratio maps.

While local differences in the raw SCI values for the different kernel sizes are observed, the result of population analysis shows a similar pattern. So, we computed the SCI values at 6

months of age for all subjects at all kernel sizes and compared these SCI maps between the different kernel sizes via correlation (see Figure 5 d). The kernel sizes were globally normalized as described above. Correlation maps of the SCI maps were very high (>0.95) across the whole brain for kernel size variations up to 4mm. We would expect higher differences for kernel sizes 5mm and above, as the scales of measurement would be significantly enlarged. And, we also see that the resulting correlations maps are highly similar across the selected kernel sizes. We then looked further into the age effect maps computed at the different kernel sizes. All kernel sizes, here, were corrected as proposed above using global hemisphere kernel size normalization at 6 months and local kernel size normalization at older ages. The results in Figure 5 e show that the age effect maps look highly similar across the different kernel sizes.

In summary, while the results in Figure 5 show that the proposed SCI is sensitive to the choice of the kernel size, the relative magnitude of SCI is highly stable within kernel size differences of 0.5mm, and the age effect results of our longitudinal study are stable across even larger kernel size differences. Based on these results, we feel that the proposed SCI should be considered stable, with respect to the choice of the kernel size within a limited range.

Discussion

Local shape complexity Index (SCI)

This paper introduces a novel method called shape complexity index for the quantification of local cortical shape. The SCI maps show that wide sulcal fundal regions display the lowest levels of local complexity, whereas several gyral walls and narrow gyral ridges display a high level of complexity. Gyral saddle regions and wider gyral ridges display intermediate complexity levels. As concave cup and convex dome regions are located at the opposite extremes of the SI scale, these cortical locations encompassing both sulcal to gyral situations within the relatively small 3mm geodesic kernel, show largest complexity, as can be seen in these results (see Figure 3-a). In contrast, locations at deep sulci close to saddle region show lower complexity, as expected (see Figure 3-b).

The proposed SCI is reliable in a scan/rescan setting and produces stable results. In contrast to local gyrification index, the SCI does not necessitate the definition of a reference surface, such as the outer surface or cerebral hull. The proposed SCI also offers novel insights into cortical folding assessment with an intermediately sized scale (3mm) between the fine scale curvature measures (< 1mm) and the larger scale GI (>20mm).

The effect of age and sex on surface complexity in the first 2 years of life

The morphological development of the human brain does not fully mature until late in childhood as measured by cortical thickness (Shaw et al., 2008; Sowell et al., 2004; 2003), by surface area (Hill et al., 2010) or by the gyrification index (Dubois et al., 2008; G. Li et al., 2014; Ronan et al., 2014). The global GI significantly increases in the left (slope=0.0167) and the right hemisphere (slope=0.0314) from 6 month to 24 month (Figure 11). The major sulci emerge in the third trimester. While almost all secondary sulci are

present at gestational week 32 as well as highly variable tertiary sulci are present by gestational week 36 or the early postnatal period, minor restructuring occurs up to age 8 years (Lohmann et al., 1999; Welker, 1990). The onset of primary, secondary and tertiary sulci results in major changes of cortical complexity. Furthermore, regional patterns of cortical surface change in the postnatal period are main factors that differentiate the human brain from other primates (Mueller et al., 2013). For example, rapid cortical changes in the temporal-parietal junction and cingulate sulcal region are related to high order cognitive functioning (Mueller et al., 2013), whereas comparative slow cortical changes are found in precentral gyrus, superior frontal and inferior temporal/temporal tip (G. Li et al., 2014). In this study, we provide further evidence for changes in local cortical surface complexity from between the 6 months to 2 years of age. The observed longitudinal patterns indicate that we should expect further increases in local surface complexity beyond 2 years of age.

In recent years, sulcal pits and gyral ridges have been hypothesized to be sources of cortical folding change, with the frequency of the major sulcal pits being stable postnatally (Im et al., 2010; Meng et al., 2014). The SCI based results presented here show a regional pattern of increased complexity close to the previously detected secondary or tertiary sulcus and gyral ridges. Figure 12 shows an example of increased SCI within the supramarginal gyrus region in a selected subject.

The inferior temporal lobe has relatively shallow sulci and large surface ratio comparing total surface area (J.-J. Kim et al., 2000; Toro et al., 2008), consisting mainly of the parahippocampal gyrus, the lateral occipitotemporal gyrus, and the medial occipitotemporal gyrus. Even though these gyri appear relatively late, at about 30 weeks gestational age (Chi et al., 1977), the inferior temporal region decreases in cortical thickness after the postnatal toddler period (approximately age 4~5) (Shaw et al., 2008). Additionally, areal expansion in these regions is low in the early postnatal period (Hill et al., 2010; G. Li et al., 2014). Here, our SCI shows a stable surface complexity in the inferior temporal lobe between the ages of 6 months to 2 years, indicating that while surface area continues to increase at a low rate in this age period, local folding complexity does not.

Most studies of the effect on sex on brain structure investigate periods later than early childhood (Creze et al., 2014; Luders et al., 2004). Consequently, the differences in developmental trajectories in the early postnatal phase (age 0~2) remain largely unclear. Recently, Li et al (2014) showed that male subjects exhibit larger localized GI values than females as neonates and at 2 years of age, in a cross-sectional analysis of the left paracentral and precuneus cortex, but without significant differences at 1 year. In our study, we also found concurring evidence that the male cortical surface is more complex than the female cortex at 6 months of age, though in different cortical regions. In our study, we found increased complexity change rates in females in the insula, middle cingulate, parieto-occipital sulcal, and right Broca's region. Additionally, our cross-sectional results show higher complexity in the lateral prefrontal, occipital, and temporal regions of females at 2 years of age. These differences between our sulcal complexity findings and Li et al's local GI findings are likely due to methodological differences, as well as different viewpoints of scale between GI (large scale) and sulcal complexity (small/medium scale). Our results provide evidence that males show higher cortical complexity early on, but females show

higher complexity later in development. Our findings suggest that higher complexity in females arises in the second year of life. These findings complement earlier findings that male infant brains show increased growth rates during the first 3 months (Holland et al., 2014), and at a later stage, adult females present greater cortical folding complexity in frontal and parietal regions, as measured via GI and the sulcation index (Dubois et al., 2008; Luders et al., 2004).

The relationship between shape complexity and tangential expansion/intrinsic curvature

Intrinsic curvature is a measurement often employed to investigate the tangential expansion of the cerebral cortex (Ronan et al., 2014; 2012). The underlying hypothesis in developmental studies is that cortical folding can be captured by locally measured tangential surface expansion. However, the morphological changes due to developmental processes are not directly described by local changes of intrinsic curvature. For example, a local widening of a sulcal or a gyral region will lead to different results, depending on the geometric setting, with reduced values in deep sulcal cup and gyral top settings and increased values in most sulcal valleys and deeper gyral ridges. In general, the interpretation of local effects can be quite difficult, and a process leading to a more folded or complex surface can yield positive or negative changes of intrinsic curvature, depending on the local setting.

The age effect results in our data analyzed via their local intrinsic curvature (Figure S8). Tangential expansion decreased bilaterally in the central sulcal, the superior frontal gyrus, the orbitofrontal cortex, and the lingual gyrus region. In contrast, a positive age correlation was observed in the posterior cingulate gyrus region, as well as in portions of the lateral temporal and parietal lobes. While these results are difficult to interpret, the reduced tangential expansion is more closely located to early maturing major sulci, whereas regions of late maturation are more likely to show positive tangential expansion (Hill et al., 2010; G. Li et al., 2014).

Next, we investigated the correlation between our novel surface complexity measure and intrinsic curvature to illustrate how the results differ. Over a large part of the brain, the two measures were correlated overall (either positively or negatively) (Figure S9). The regions of significant positive correlation contain deep sulci or major gyri, such as the superior temporal gyrus, the cingulate gyrus, and a portion of pre- and post-central sulcal regions. On the other hand, the negative correlation appears in the insula, portions of occipital lobe (spanning primary visual cortex), and the orbitofrontal region with relatively different shapes (Jang et al., 2006; Regis et al., 2005). The regions with a positive correlation between SCI and intrinsic curvature may be increasing in complexity due to tangential surface expansion which may be due to evolutionary pressure from additional mitotic rounds of the proliferative neuronal precursor pool, as captured by leading (evolutionary) hypotheses of expanded cortical areas (Rakic, 1995). In contrast, regions with a negative correlation may show higher complexity (as compared to intrinsic curvature) due to development of secondary and tertiary sulci, and sulcal pits or additional gyral branches (Hill et al., 2010).

Finally, we observe that a number of regions with a strong age association for the intrinsic curvature are not present in the correlation map. Furthermore, some regions of high correlation between SCI and intrinsic curvature are not shown in the age effect map using

the intrinsic curvature. This further indicates that our novel measure captures a shape perspective that is complementary and more intuitive comparing to intrinsic curvature.

Conclusion

In this paper, we propose a novel method to calculate local cortical surface shape complexity that does not require a reference simplified surface model. The measure captures local shape changes mainly within a single sulcal or gyral region, which allows us to discriminate the widening (reduced SCI) versus deepening (non-reduced SCI) of regions, as well as to identify regions with developing secondary and tertiary sulci. The proposed SCI does not aim to capture any particular cortical region more efficiently. Our experimental results do not indicate that there is such a location specific sensitivity in capturing changes of SCI across the cortical surface.

Our quantitative complexity study of cortical shape changes in early development using this metric shows a regionally specific pattern over the age and the difference of sexually dimorphic pattern. In contrast to other methods, the local measure presented quantifies complexity at the intermediate local scale (of 3mm at 6 months of age). It is noteworthy that the results presented here are the first to take into account localized brain surface growth and inter-subject size differences via an adaptive geodesic kernel size. This local correction accounts for non-uniform surface growth over time into the analysis.

To our knowledge, this is the first longitudinal study of surface complexity development in the first two years of life, at an intermediate scale that does not span multiple sulci or gyri. We found that the local SCI is highly correlated with age. We also found sexual dimorphisms in the insula, middle cingulate, parieto-occipital sulcal and in Broca's region.

Supplementary Material

Refer to Web version on PubMed Central for supplementary material.

Acknowledgments

References

Armstrong E, Schleicher A, Omran H, Curtis M, Zilles K. The Ontogeny of Human Gyrification. Cereb. Cortex. 1995; 5:56–63. doi:10.1093/cercor/5.1.56. [PubMed: 7719130]

Avants BB, Epstein CL, Grossman M, Gee JC. Symmetric diffeomorphic image registration with cross-correlation: evaluating automated labeling of elderly and neurodegenerative brain. Med Image Anal. 2008; 12:26–41. doi:10.1016/j.media.2007.06.004. [PubMed: 17659998]

Benjamini Y, Hochberg Y. Controlling the false discovery rate: a practical and powerful approach to multiple testing. J. Roy. Statist. Soc. Ser. B. 1995; 57:289–300.

Bryson SE, Zwaigenbaum L, McDermott C, Rombough V, Brian J. The Autism Observation Scale for Infants: scale development and reliability data. J Autism Dev Disord. 2008; 38:731–738. doi:10.1007/s10803-007-0440-y. [PubMed: 17874180]

Chi JG, Dooling EC, Gilles FH. Gyral development of the human brain. Ann. Neurol. 1977; 1:86–93. doi:10.1002/ana.410010109. [PubMed: 560818]

Chung MK, Robbins SM, Dalton KM, Davidson RJ, Alexander AL, Evans AC. Cortical thickness analysis in autism with heat kernel smoothing. Neuroimage. 2005; 25:1256–1265. doi:10.1016/j.neuroimage.2004.12.052. [PubMed: 15850743]

Chung MK, Worsley KJ, Nacewicz BM, Dalton KM, Davidson RJ. General multivariate linear modeling of surface shapes using SurfStat. Neuroimage. 2010; 53:491–505. doi:10.1016/j.neuroimage.2010.06.032. [PubMed: 20620211]

Cohen-Steiner, D.; Morvan, J-M. Approximation of Normal Cycles. 2003.

Collins DL, Neelin P, Peters TM, Evans AC. Automatic 3D intersubject registration of MR volumetric data in standardized Talairach space. J Comput Assist Tomogr. 1994; 18:192–205. [PubMed: 8126267]

Creze M, Versheure L, Besson P, Sauvage C, Leclerc X, Jissendi-Tchofo P. Age- and gender-related regional variations of human brain cortical thickness, complexity, and gradient in the third decade. Hum Brain Mapp. 2014; 35:2817–2835. doi:10.1002/hbm.22369. [PubMed: 24142374]

Dierker DL, Feczko E, Pruett JR, Petersen SE, Schlaggar BL, Constantino JN, Harwell JW, Coalson TS, Van Essen DC. Analysis of cortical shape in children with simplex autism. Cereb. Cortex. 2015; 25:1042–1051. doi:10.1093/cercor/bht294. [PubMed: 24165833]

Dubois J, Benders M, Cachia A, Lazeyras F, Ha-Vinh Leuchter R, Sizonenko SV, Borradori-Tolsa C, Mangin JF, Hüppi PS. Mapping the early cortical folding process in the preterm newborn brain. Cereb. Cortex. 2008; 18:1444–1454. doi:10.1093/cercor/bhm180. [PubMed: 17934189]

Fonov V, Evans AC, Botteron K, Almli CR, McKinstry RC, Collins DL. Unbiased average age-appropriate atlases for pediatric studies. Neuroimage. 2011; 54:313–327. doi:10.1016/j.neuroimage.2010.07.033. [PubMed: 20656036]

Fonov, VS.; Janke, A.; Caramanos, Z.; Arnold, DL.; Narayanan, S.; Pike, GB.; Collins, DL. Medical Imaging and Augmented Reality, Lecture Notes in Computer Science. Springer Berlin Heidelberg; Berlin, Heidelberg: 2010. Improved Precision in the Measurement of Longitudinal Global and Regional Volumetric Changes via a Novel MRI Gradient Distortion Characterization and Correction Technique; p. 324-333.doi:10.1007/978-3-642-15699-1_34

Free SL, Sisodiya SM, Cook MJ, Fish DR, Shorvon SD. Three-dimensional fractal analysis of the white matter surface from magnetic resonance images of the human brain. Cereb. Cortex. 1996; 6:830–836. [PubMed: 8922340]

Gaser C, Luders E, Thompson PM, Lee AD, Dutton RA, Geaga JA, Hayashi KM, Bellugi U, Galaburda AM, Korenberg JR, Mills DL, Toga AW, Reiss AL. Increased local gyrification mapped in Williams syndrome. Neuroimage. 2006; 33:46–54. doi:10.1016/j.neuroimage.2006.06.018. [PubMed: 16901723]

Gouttard S, Styner M, Prastawa M, Piven J, Gerig G. Assessment of reliability of multi-site neuroimaging via traveling phantom study. Med Image Comput Comput Assist Interv. 2008; 11:263–270. [PubMed: 18982614]

Hazlett HC, Gu H, McKinstry RC, Shaw DWW, Botteron KN, Dager SR, Styner M, Vachet C, Gerig G, Paterson SJ, Schultz RT, Estes AM, Evans AC, Piven J, Network I. Brain Volume Findings in 6-Month-Old Infants at High Familial Risk for Autism. Am J Psychiatry. 2012; 169:601–608. doi:10.1176/appi.ajp.2012.11091425. [PubMed: 22684595]

Hill J, Inder T, Neil J, Dierker D, Harwell J, Van Essen D. Similar patterns of cortical expansion during human development and evolution. Proc. Natl. Acad. Sci. U.S.A. 2010; 107:13135–13140. doi:10.1073/pnas.1001229107. [PubMed: 20624964]

Holland D, Chang L, Ernst TM, Curran M, Buchthal SD, Alicata D, Skranes J, Johansen H, Hernandez A, Yamakawa R, Kuperman JM, Dale AM. Structural Growth Trajectories and Rates of Change in the First 3 Months of Infant Brain Development. JAMA Neurol. 2014; 71:1266–1274. doi: 10.1001/jamaneurol.2014.1638. [PubMed: 25111045]

Hosking J. On the characterization of distributions by their L-moments. Journal of Statistical Planning and Inference. 2006; 136:193–198. doi:10.1016/j.jspi.2004.06.004.

Hudziak JJ, Albaugh MD, Ducharme S, Karama S, Spottswood M, Crehan E, Evans AC, Botteron KN, Grp BDC. Cortical Thickness Maturation and Duration of Music Training: Health-Promoting Activities Shape Brain Development. J Am Acad Child Adolesc Psychiatry. 2014; 53:1153–1161. doi:10.1016/j.jaac.2014.06.015. [PubMed: 25440305]

Im K, Jo HJ, Mangin J-F, Evans AC, Kim SI, Lee J-M. Spatial Distribution of Deep Sulcal Landmarks and Hemispherical Asymmetry on the Cortical Surface. Cereb. Cortex. 2010; 20:602–611. doi: 10.1093/cercor/bhp127. [PubMed: 19561060]

Jang D-P, Kim J-J, Chung T-S, An SK, Jung YC, Lee J-K, Lee J-M, Kim I-Y, Kim SI. Shape deformation of the insula in schizophrenia. Neuroimage. 2006; 32:220–227. doi:10.1016/j.neuroimage.2006.01.032. [PubMed: 16730197]

Kim J-J, Crespo-Facorro B, Andreasen NC, O'Leary DS, Zhang B, Harris G, Magnotta VA. An MRI-Based Parcellation Method for the Temporal Lobe. Neuroimage. 2000; 11:271–288. doi:10.1006/nimg.2000.0543. [PubMed: 10725184]

Kim JS, Singh V, Lee JK, Lerch J, Ad-Dab'bagh Y, MacDonald D, Lee JM, Kim SI, Evans AC. Automated 3-D extraction and evaluation of the inner and outer cortical surfaces using a Laplacian map and partial volume effect classification. Neuroimage. 2005; 27:210–221. doi:10.1016/j.neuroimage.2005.03.036. [PubMed: 15896981]

KIM SH, Fonov V, Collins DL, Gerig G, Styner MA. Shape index distribution based local surface complexity applied to the human cortex. SPIE Medical Imaging. 2015; 9413:941344–941344–8. doi:10.1117/12.2081560.

KIM SH, Fonov VS, Dietrich C, Vachet C, Hazlett HC, Smith RG, Graves MM, Piven J, Gilmore JH, Dager SR, McKinstry RC, Paterson S, Evans AC, Collins DL, Gerig G, Styner MA, Network I. Adaptive prior probability and spatial temporal intensity change estimation for segmentation of the one-year-old human brain. J. Neurosci. Methods. 2013; 212:43–55. doi:10.1016/j.jneumeth.2012.09.018. [PubMed: 23032117]

Kochunov P, Castro C, Davis D, Dudley D, Brewer J, Zhang Y, Kroenke CD, Purdy D, Fox PT, Simerly C, Schatten G. Mapping primary gyrogenesis during fetal development in primate brains: high-resolution in utero structural MRI of fetal brain development in pregnant baboons. Front Neurosci. 2010; 4:20. doi:10.3389/fnins.2010.00020. [PubMed: 20631812]

Koenderink JJ, van Doorn AJ. Surface shape and curvature scales. Image and vision computing. 1992 doi:10.1016/0262-8856(92)90076-F.

Koran MEI, Hohman TJ, Edwards CM, Vega JN, Pryweller JR, Slosky LE, Crockett G, de Rey LV, Meda SA, Dankner N, Avery SN, Blackford JU, Dykens EM, Thornton-Wells TA. Differences in age-related effects on brain volume in Down syndrome as compared to Williams syndrome and typical development. J Neurodev Disord 6. 2014 doi:10.1186/1866-1955-6-8.

Lange N, Travers BG, Bigler ED, Prigge MBD, Froehlich AL, Nielsen JA, Cariello AN, Zielinski BA, Anderson JS, Fletcher PT, Alexander AA, Lainhart JE. Longitudinal volumetric brain changes in autism spectrum disorder ages 6-35 years. Autism Res. 2015; 8:82–93. doi:10.1002/aur.1427. [PubMed: 25381736]

Lefèvre J, Germanaud D, Dubois J, Rousseau F, de Macedo Santos I, Angleys H, Mangin J-F, Hüppi PS, Girard N, De Guio F. Are Developmental Trajectories of Cortical Folding Comparable Between Cross-sectional Datasets of Fetuses and Preterm Newborns? Cereb. Cortex. 2015:bhv123. doi:10.1093/cercor/bhv123.

Li G, Wang L, Shi F, Lyall AE, Lin W, Gilmore JH, Shen D. Mapping longitudinal development of local cortical gyrification in infants from birth to 2 years of age. J. Neurosci. 2014; 34:4228–4238. doi:10.1523/JNEUROSCI.3976-13.2014. [PubMed: 24647943]

Li K, Guo L, Li G, Nie J, Faraco C, Cui G, Zhao Q, Miller LS, Liu T. Gyral folding pattern analysis via surface profiling. Neuroimage. 2010; 52:1202–1214. doi:10.1016/j.neuroimage.2010.04.263. [PubMed: 20472071]

Lohmann G, Cramon, von DY, Steinmetz H. Sulcal variability of twins. Cereb. Cortex. 1999; 9:754–763. doi:10.1093/cercor/9.4.392. [PubMed: 10554998]

Luders E, Narr KI, Thompson PM, Rex DE, Jancke L, Steinmetz H, Toga AW. Gender differences in cortical complexity. Nat. Neurosci. 2004; 7:799–800. doi:10.1038/nn1277. [PubMed: 15338563]

Lui JH, Hansen DV, Kriegstein AR. Development and Evolution of the Human Neocortex. Cell. 2011; 146:18–36. doi:10.1016/j.cell.2011.06.030. [PubMed: 21729779]

Lyttelton O, Boucher M, Robbins S, Evans A. An unbiased iterative group registration template for cortical surface analysis. Neuroimage. 2007; 34:1535–1544. doi:10.1016/j.neuroimage. 2006.10.041. [PubMed: 17188895]

Marcus Jenkins JV, Woolley DP, Hooper SR, De Bellis MD. Direct and Indirect Effects of Brain Volume, Socioeconomic Status and Family Stress on Child IQ. J Child Adolesc Behav. 2013; 1

Meng Y, Li G, Lin W, Gilmore JH, Shen D. Spatial distribution and longitudinal development of deep cortical sulcal landmarks in infants. Neuroimage. 2014; 100:206–218. doi:10.1016/j.neuroimage. 2014.06.004. [PubMed: 24945660]

Mueller S, Wang D, Fox MD, Yeo BTT, Sepulcre J, Sabuncu MR, Shafee R, Lu J, Liu H. Individual Variability in Functional Connectivity Architecture of the Human Brain. Neuron. 2013; 77:586–595. doi:10.1016/j.neuron.2012.12.028. [PubMed: 23395382]

Rakic P. A small step for the cell, a giant leap for mankind: a hypothesis of neocortical expansion during evolution. Trends Neurosci. 1995; 18:383–388. [PubMed: 7482803]

Regis J, Mangin JF, Ochiai T, Frouin V, Riviere D, Cachia A, Tamura M, Samson Y. "Sulcal root" generic model: a hypothesis to overcome the variability of the human cortex folding patterns. Neurol. Med. Chir. (Tokyo). 2005; 45:1–17. doi:10.2176/nmc.45.1. [PubMed: 15699615]

Rettmann ME, Kraut MA, Prince JL, Resnick SM. Cross-sectional and longitudinal analyses of anatomical sulcal changes associated with aging. Cereb. Cortex. 2006; 16:1584–1594. doi: 10.1093/cercor/bhj095. [PubMed: 16400155]

Robbins S, Evans AC, Collins DL, Whitesides S. Tuning and comparing spatial normalization methods. Med Image Anal. 2004; 8:311–323. doi:10.1016/j.media.2004.06.009. [PubMed: 15450225]

Ronan L, Voets N, Rua C, Alexander-Bloch A, Hough M, Mackay C, Crow TJ, James A, Giedd JN, Fletcher PC. Differential Tangential Expansion as a Mechanism for Cortical Gyrification. Cereb. Cortex. 2014; 24:2219–2228. doi:10.1093/cercor/bht082. [PubMed: 23542881]

Ronan L, Voets NL, Hough M, Mackay C, Roberts N, Suckling J, Bullmore ET, James A, Fletcher PC. Consistency and interpretation of changes in millimeter-scale cortical intrinsic curvature across three independent datasets in schizophrenia. Neuroimage. 2012; 63:611–621. doi:10.1016/j.neuroimage.2012.06.034. [PubMed: 22743195]

Rubner Y, Tomasi C, Guibas LJ. The Earth Mover's Distance as a Metric for Image Retrieval. International Journal of Computer Vision. 2000; 40:99–121. doi:10.1023/A:1026543900054.

Schaer M, Cuadra MB, Tamarit L, Lazeyras F, Eliez S, Thiran J-P. A surface-based approach to quantify local cortical gyrification. IEEE Trans Med Imaging. 2008; 27:161–170. doi:10.1109/TMI.2007.903576. [PubMed: 18334438]

Shaw P, Kabani NJ, Lerch JP, Eckstrand K, Lenroot R, Gogtay N, Greenstein D, Clasen L, Evans A, Rapoport JL, Giedd JN, Wise SP. Neurodevelopmental trajectories of the human cerebral cortex. J. Neurosci. 2008; 28:3586–3594. doi:10.1523/JNEUROSCI.5309-07.2008. [PubMed: 18385317]

Sled JG, Zijdenbos AP, Evans AC. A nonparametric method for automatic correction of intensity nonuniformity in MRI data. IEEE Trans Med Imaging. 1998; 17:87–97. doi:10.1109/42.668698. [PubMed: 9617910]

Sowell ER, Peterson BS, Thompson PM, Welcome SE, Henkenius AL, Toga AW. Mapping cortical change across the human life span. Nat. Neurosci. 2003; 6:309–315. doi:10.1038/nn1008. [PubMed: 12548289]

Sowell ER, Thompson PM, Leonard CM, Welcome SE, Kan E, Toga AW. Longitudinal mapping of cortical thickness and brain growth in normal children. J. Neurosci. 2004; 24:8223–8231. doi: 10.1523/JNEUROSCI.1798-04.2004. [PubMed: 15385605]

Sowell ER, Trauner DA, Gamst A, Jernigan TL. Development of cortical and subcortical brain structures in childhood and adolescence: a structural MRI study. Dev Med Child Neurol. 2002; 44:4–16. [PubMed: 11811649]

Stone J, Bray A. A learning rule for extracting spatio-temporal invariances. Network: Computation in Neural Systems. 1995; 6:429–436. doi:10.1088/0954-898X_6_3_008.

Storey JD, Taylor JE, Siegmund D. Strong control, conservative point estimation and simultaneous conservative consistency of false discovery rates: a unified approach. Journal of the Royal Statistical Society Series B-Statistical Methodology. 2004; 66:187–205. doi:10.1111/j. 1467-9868.2004.00439.x.

Storsve AB, Fjell AM, Tamnes CK, Westlye LT, Overbye K, Aasland HW, Walhovd KB. Differential Longitudinal Changes in Cortical Thickness, Surface Area and Volume across the Adult Life Span: Regions of Accelerating and Decelerating Change. J. Neurosci. 2014; 34:8488–8498. doi:10.1523/JNEUROSCI.0391-14.2014. [PubMed: 24948804]

Su S, White T, Schmidt M, Kao C-Y, Sapiro G. Geometric computation of human gyrification indexes from magnetic resonance images. Hum Brain Mapp. 2013; 34:1230–1244. doi:10.1002/hbm. 21510. [PubMed: 22331577]

Toro R, Perron M, Pike B, Richer L, Veillette S, Pausova Z, Paus T. Brain size and folding of the human cerebral cortex. Cereb. Cortex. 2008; 18:2352–2357. doi:10.1093/cercor/bhm261. [PubMed: 18267953]

Van Leemput K, Maes F, Vandermeulen D, Suetens P. Automated model-based tissue classification of MR images of the brain. IEEE Trans Med Imaging. 1999; 18:897–908. doi:10.1109/42.811270. [PubMed: 10628949]

Welker, W. Cerebral Cortex, Cerebral Cortex. Springer US; Boston, MA: 1990. Why Does Cerebral Cortex Fissure and Fold?; p. 3-136.doi:10.1007/978-1-4615-3824-0_1

Wright R, Kyriakopoulou V, Ledig C, Rutherford MA, Hajnal JV, Rueckert D, Aljabar P. Automatic quantification of normal cortical folding patterns from fetal brain MRI. Neuroimage. 2014; 91:21–32. doi:10.1016/j.neuroimage.2014.01.034. [PubMed: 24473102]

Yotter RA, Nenadic I, Ziegler G, Thompson PM, Gaser C. Local cortical surface complexity maps from spherical harmonic reconstructions. Neuroimage. 2011; 56:961–973. doi:10.1016/j.neuroimage.2011.02.007. [PubMed: 21315159]

Zielinski BA, Prigge MBD, Nielsen JA, Froehlich AL, Abildskov TJ, Anderson JS, Fletcher PT, Zygmunt KM, Travers BG, Lange N, Alexander AL, Bigler ED, Lainhart JE. Longitudinal changes in cortical thickness in autism and typical development. Brain. 2014; 137:1799–1812. doi: 10.1093/brain/awu083. [PubMed: 24755274]

ZILLES K, ARMSTRONG E, SCHLEICHER A, KRETSCHMANN HJ. The Human Pattern of Gyrification in the Cerebral-Cortex. Anat. Embryol. 1988; 179:173–179. [PubMed: 3232854]

Highlights

- Shape complexity index quantified by the distributions of local surface topology.

- The adaptive geodesic kernel captures fine differences of the local shape index distribution.

- The stability and reliability of shape complexity show using scan/rescan dataset.

- The influence of the kernel size is presented using the various kernel sizes.

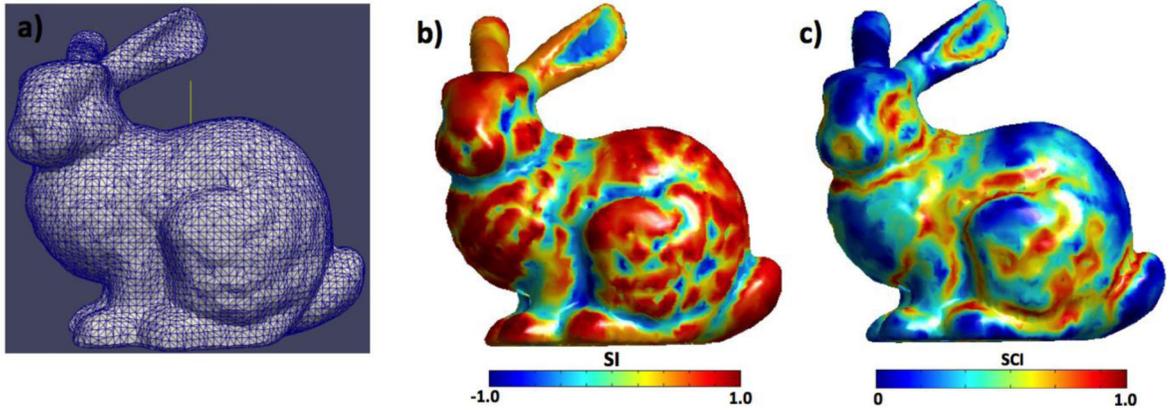- The complexity changes show a regionally specific pattern over the age.

Figure 1.
Example bunny surface model. a) Surface mesh model, b) shape index (SI) mapping on surface, c) its EMD based surface complexity map at a 3mm geodesic kernel. The regions containing both concave and convex shape show a high complexity values. In contrast, regions of similar shape index show a low complexity score. The range of complexity score is from 0 (blue color; simple) to 1.0 (red color; complex).
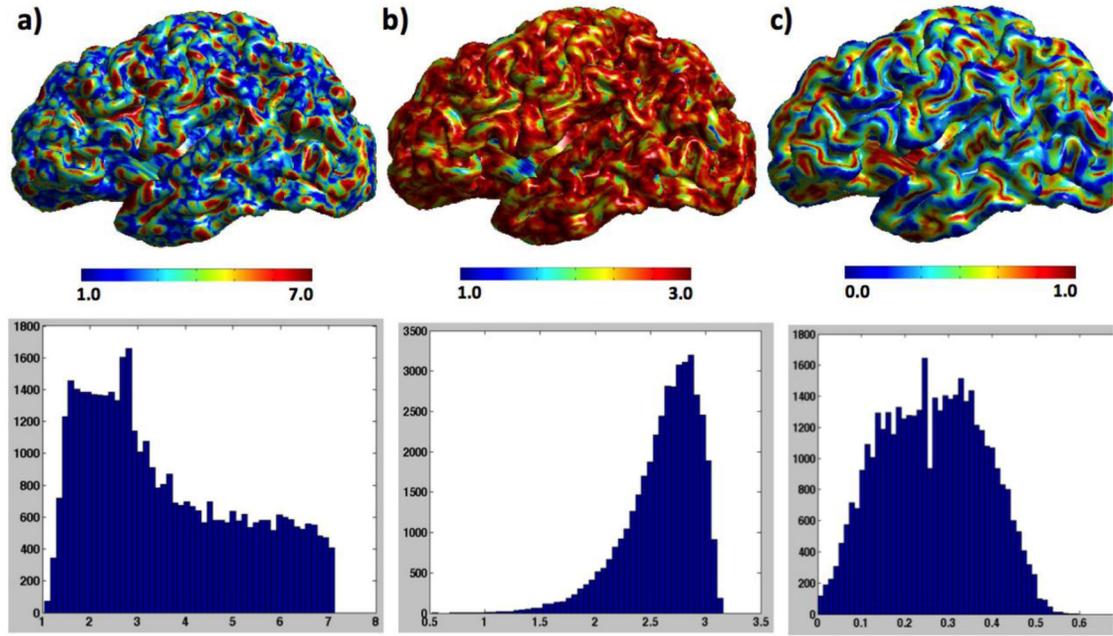
Figure 2.
Local shape complexity as calculated via kurtosis (a), entropy (b) and EMD (c) within a 3mm geodesic neighborhood. The distribution of each calculated SCI across the full brain surface is shown in the bottom row. The kurtosis based SCI is quite noisy compared to the other measures, resulting in a wide distribution over the full brain. The whole brain histogram of SCI using the entropy tends to be skewed to right side and the measure seems to have a ceiling effect with little dynamic range. The EMD based SCI measure looks both smoother, of high dynamic range and a symmetric, near Gaussian whole brain distribution.
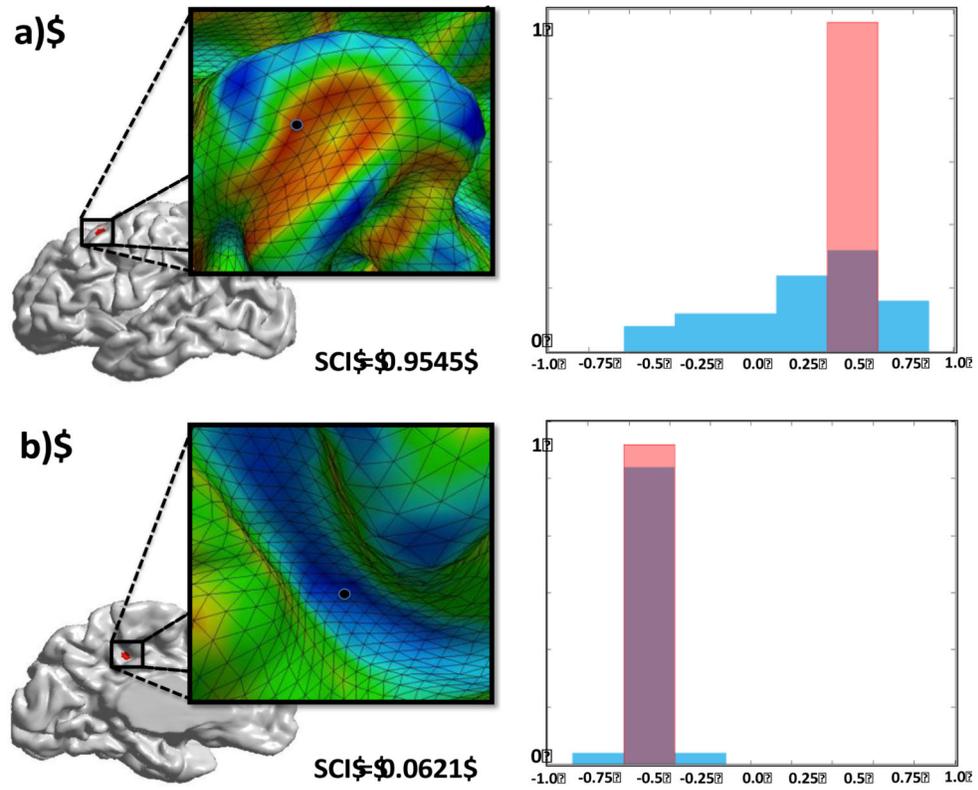
Figure 3.
Local examples of the proposed SCI: The local distributions of SI (blue color histogram) and its best fitting basic model (red color histogram: a) 7th, ridge and b) 3th, valley) at selected locations (left, vertex is indicated via a black dot). In this particular example, the gyral regions (a) shows a higher complexity than the sulcal regions (b).
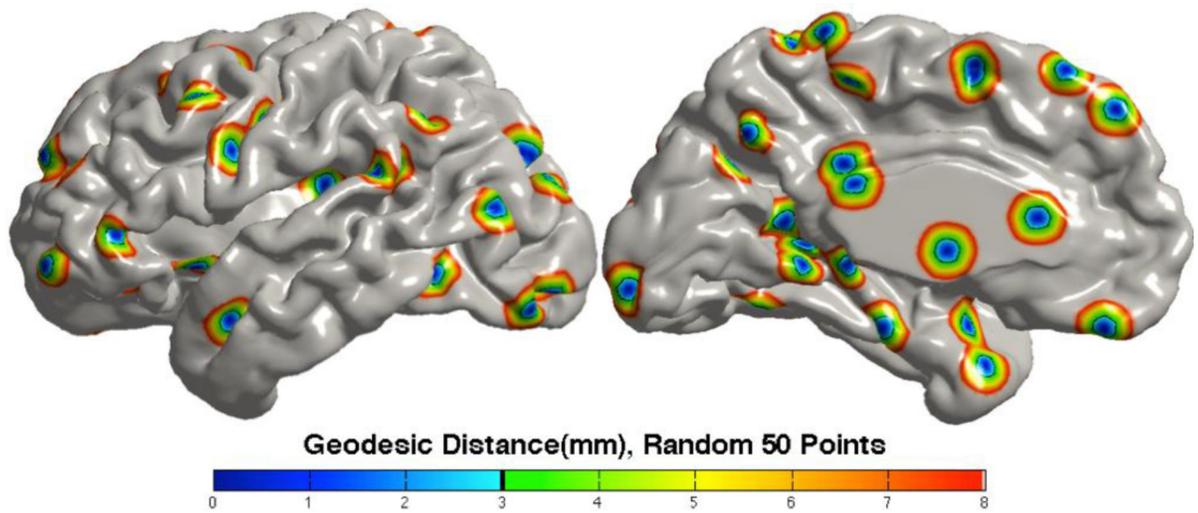
Figure 4.
The radius of different geodesic kernels is mapped on the surface model of 6-month-old brain at 50 randomly selected surface vertices. A kernel size below 3mm seems too small to detect valuable local complexity, and a kernel size beyond 5-6mm encompasses both sulcal and gyral regions.

Kernel Size

2.5mm   **3.0mm**   **3.5mm**   **4.0mm**   **8.0mm**
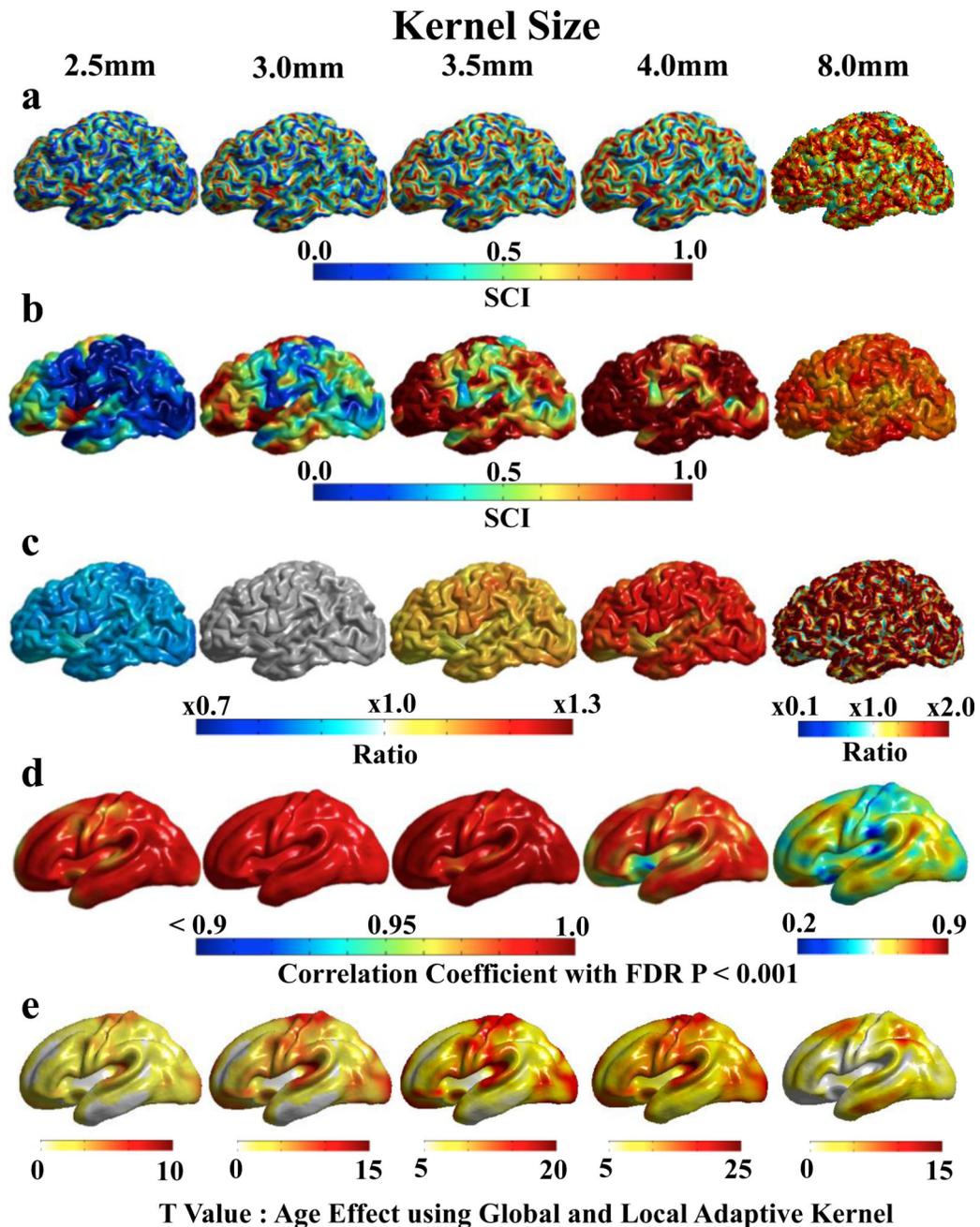
Figure 5.
The validation for different kernel size: a) shows the raw SCI with each kernel size from 2.5 mm to 4 mm and b) smoothed local SCI. Red color indicates complex and blue color indicates relatively simply shaped regions. The ratio between the smoothed SCI at 3mm (second row) and with the SCI at the other kernel sizes is show in c). The correlation map of SCIs across all 6 months datasets computed at 3mm kernel size as compared to computed with the other kernel sizes is visualized in d). The raw t-score map of the age effect calculated at all kernel sizes in e)
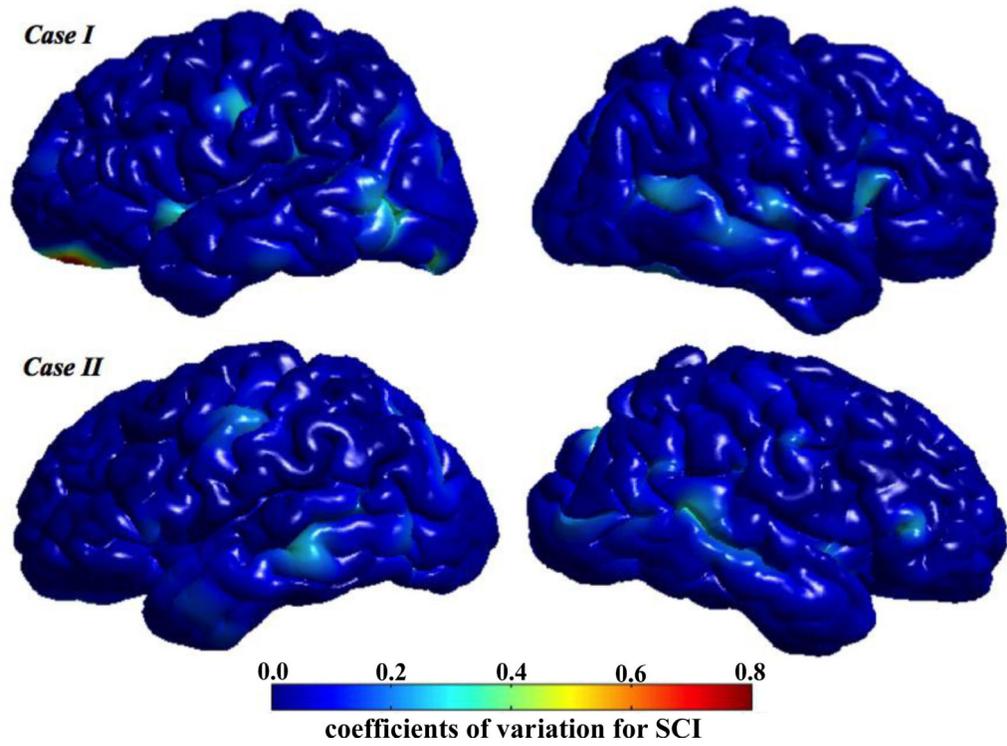
Figure 6.
Coefficients of variation for SCI maps were calculated using two sets of adult brains (Case I and Case II). Almost all regions show coefficients below 0.3%.
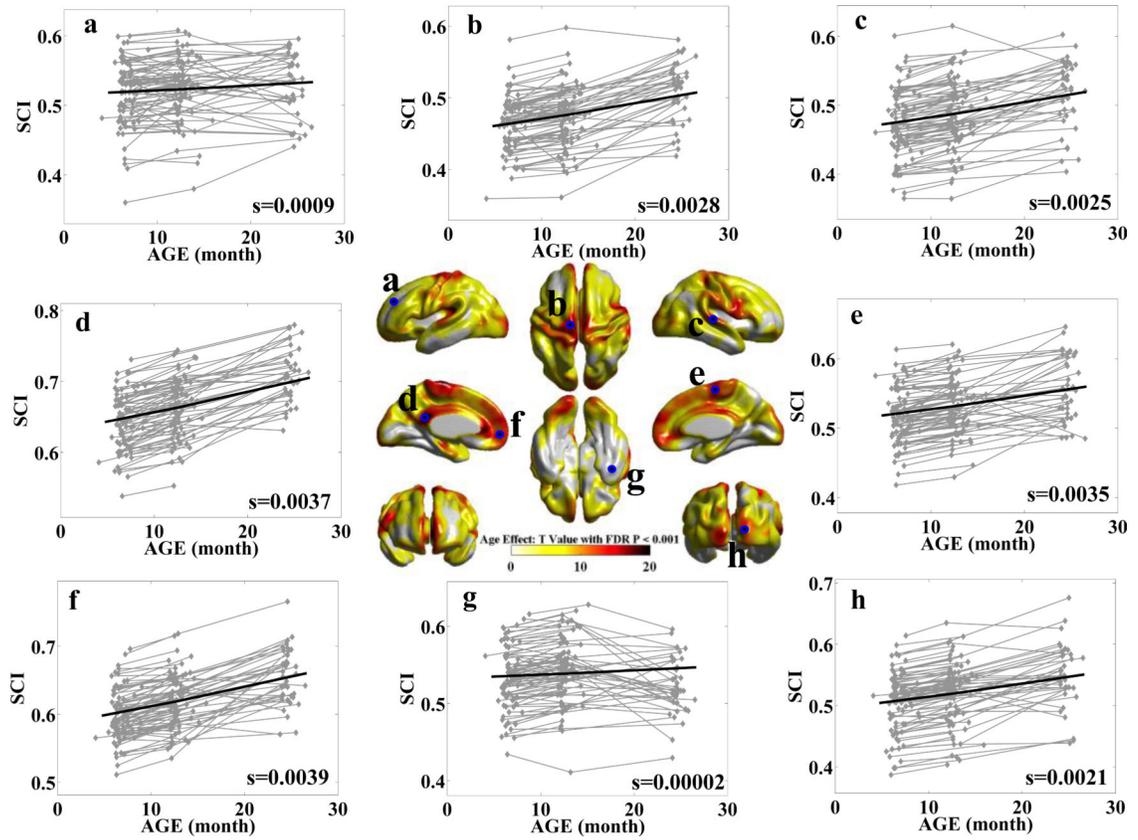
Figure 7.
The effect of age. SCI increased in almost regions except bilateral superior frontal and inferior temporal regions from 6 to 24 months of age. s is slope value using linear fitting. (See the large-scale picture of T value map also in Supplemental Figure S6):
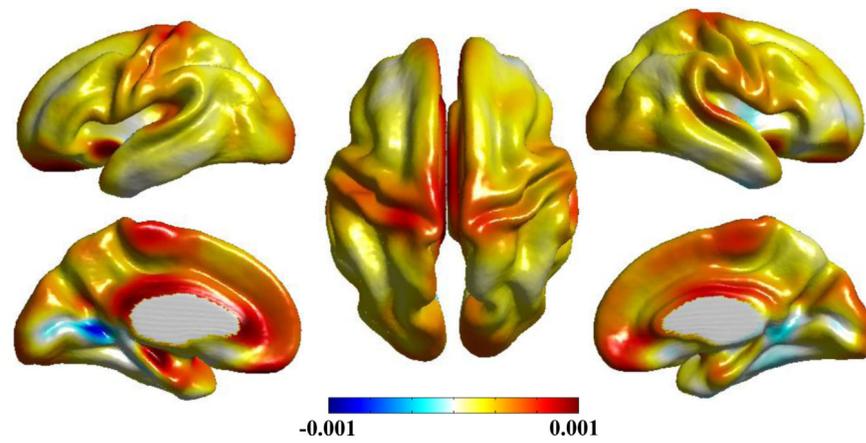
Figure 8.
The SCI change rates per month between 6 and 24 months old. The most regions show the increasing rates with mean rate 0.0005 except bilateral calcarine fissure and lingual gyrus regions. (See the piece-wise linear SCI change rates map between 6 and 12 months and between 12 and 24 months in the Supplemental Figure S7):
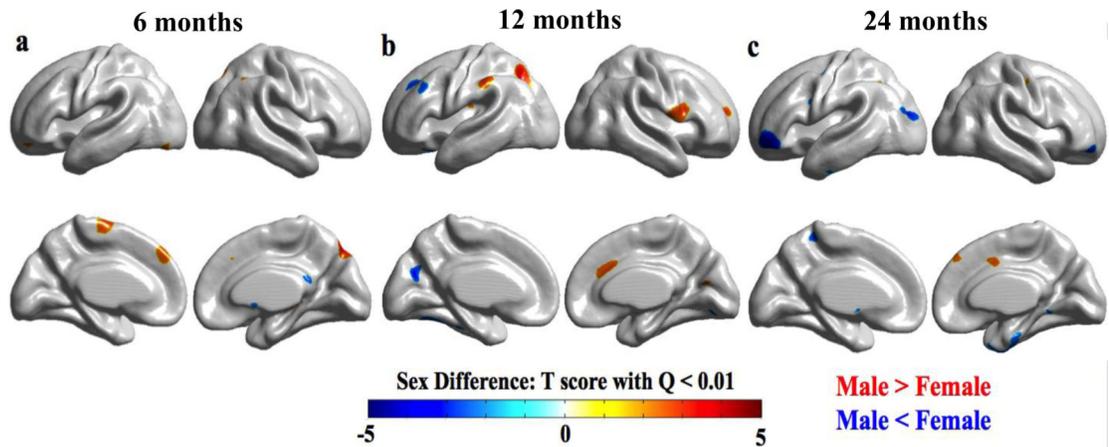
Figure 9.
The cross-sectional result of sexual dimorphisms. Male is more complex than female at 6 months of age, but the more complex regions in female does not appear in this age (a). Left superior frontal and parieto-occipital sulcal region is more complex in female, but left parietal and right anterior cingulate region shows more complex in male at 12 months (b). There is no difference regions in which sexual dimorphism appeared in 6 and 12 months of age, left prefrontal region, on the other hand, is more complex in female at 24 months (c).
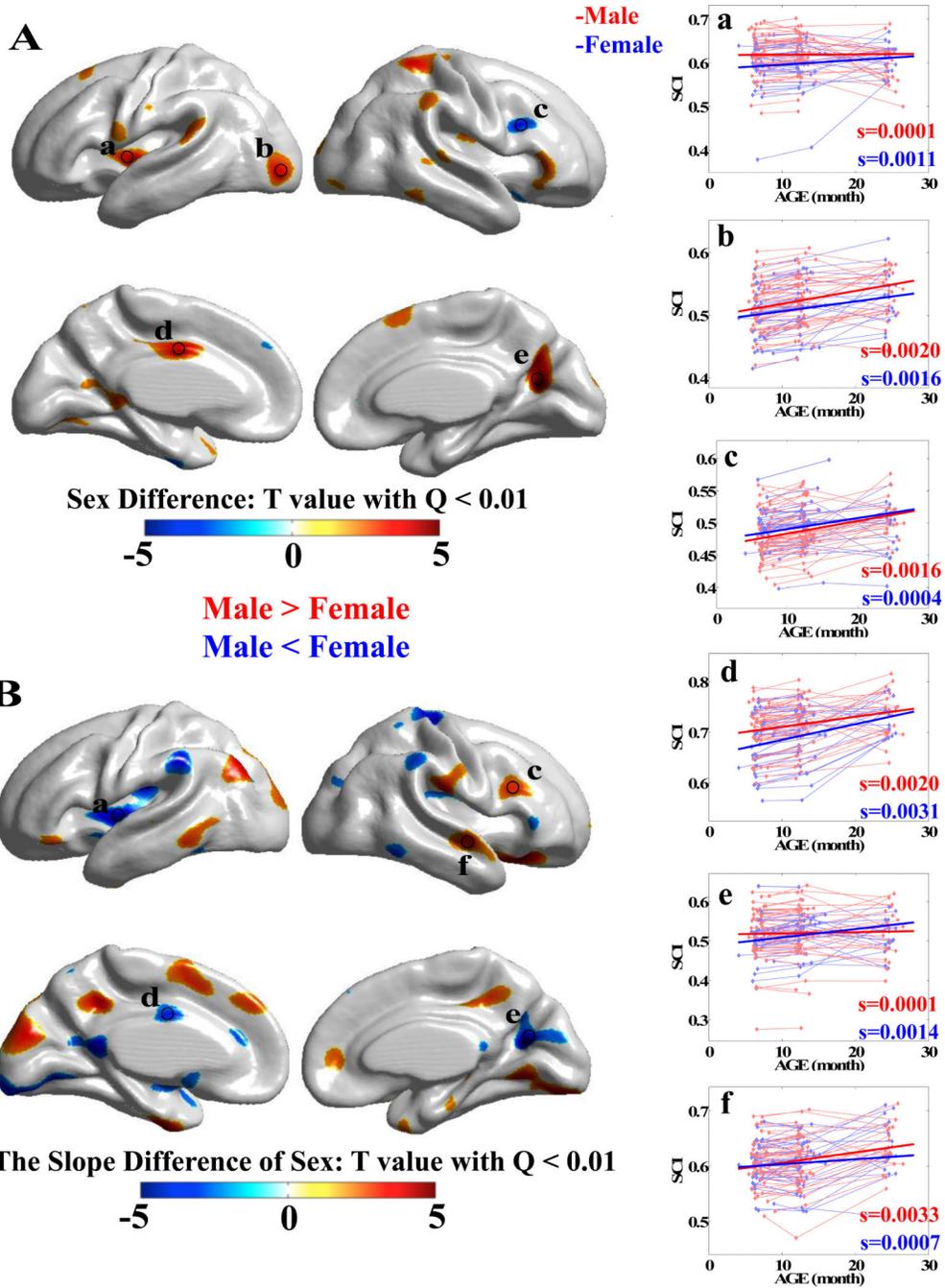
Figure 10.
The longitudinal result of sexual dimorphism. Insula (a), left visual cortex (b), middle cingulate (d) and parieto-occipital sulcal regions (e) is more complex in male, but right Broca's regions (c) is more complex in female (Figure A). The SCI change rates show in Figure B. Regions a, d and e (in which male is more complex) shows that female is fast rate of changes than male, region c (in which female is more complex), on the other hand, shows that male is fast rate of changes than female. The longitudinal scatter plot shows in right column. And s (red is male, blue is female) is slope value using linear fitting.
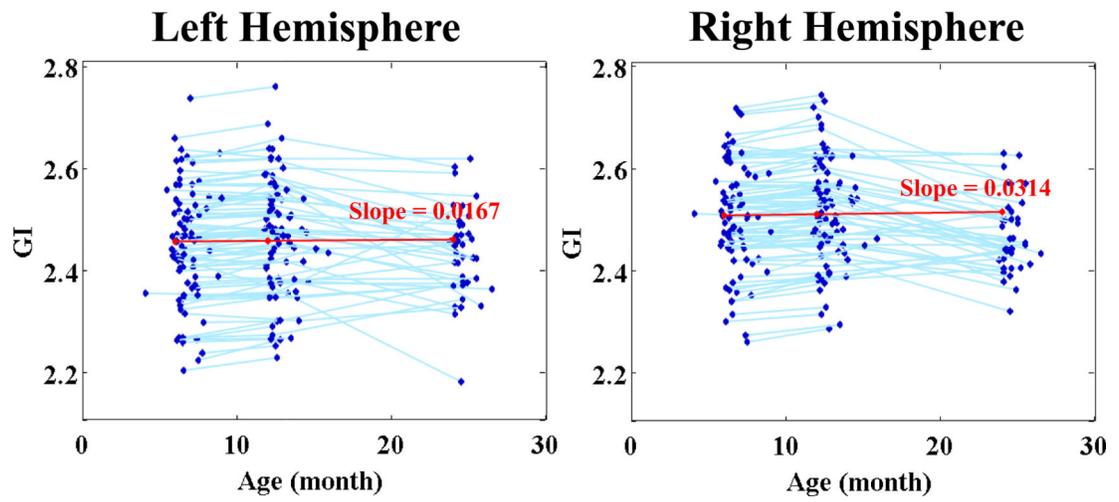
Figure 11.
The global gyrification index over the observed age, from 6 month to 24 month. Both hemisphere significantly increase (left slope 0.0167 and right slope 0.0314, p<0.01).
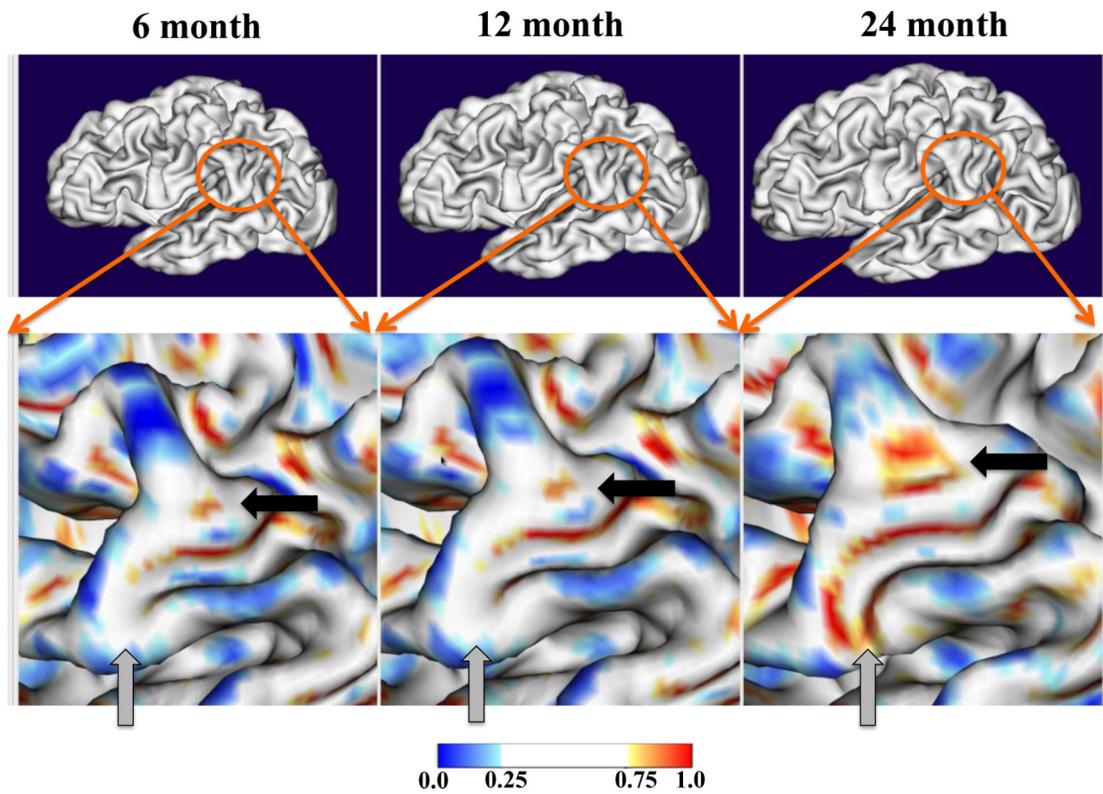
Figure 12.
The change of SCI from 6 month to 24 month in the supramarginal gyrus region in a selected subject. SCI increase here is due to an emerging non-primary sulcus in gyral ridge regions (black arrow), and a sulcus extension of an existing sulcus (gray arrow). The SCI color mapping is adjusted to highlight this particular effect.

Table 1

Demographic information

	All	**Male**	**Female**
Number of Scans	**202**	**126**	**76**
Time point 6 months (mean age ± std)	82 (6.73 ± 0.78)	52 (6.76 ± 0.74)	30 (6.67 ± 0.86)
Time point 12 months (mean age ± std)	82 (12.77 ± 0.78)	52 (12.68 ± 0.65)	30 (12.93 ± 1.00)
Time point 24 months (mean age ± std)	38 (24.64 ± 0.58)	22 (24.69 ± 0.64)	16 (24.59 ± 0.49)